Hindawi
Mathematical Problems in Engineering
Volume 2018, Article ID 4128520, 10 pages
https://doi.org/10.1155/2018/4128520

Research Article

Structure Design and Kinematics Analysis of a Novel Unpowered Load-Carrying Lower Extremity Exoskeleton with Parallel Topology

Qiang Yan, Jianjun Zhang, and Kaicheng Qi

Hebei Province Parallel Equipment Research Laboratory, Hebei University of Technology, Tianjin, China

Correspondence should be addressed to Jianjun Zhang; zhjjun96@139.com

Received 15 June 2018; Revised 9 August 2018; Accepted 9 September 2018; Published 25 September 2018

Academic Editor: Alberto Borboni

A novel unpowered load-carrying parallel lower extremity exoskeleton is proposed. It is aimed at enhancing the load-bearing ability of the operator. Firstly, the structure of the novel exoskeleton is depicted in the second section; meanwhile, the degree of freedom concerning the exoskeleton is gotten by analyzing the number of links and the kinematic joints. Secondly, the forward position analysis of the exoskeleton for the swing leg is obtained. Using the expressions concerning the joints of knee and angle, the workspace of the swing leg in supporting gait circle is analyzed by the software of MATLAB. Thirdly, according to the schematic diagram of the mechanism, the static force analysis of the supporting leg for the exoskeleton is obtained. Finally, the static force of the supporting leg of the person who is not wearing the unpowered exoskeleton is gotten. Meanwhile, the genetic algorithm is used to get the optimum stiffness of the spring for energy-restoring device. By comparing the changes of force and torque for the supporting leg who is not wearing it and the skeleton which is worn by a person, some conclusions are carried out.

1. Introduction

The load-carrying lower limb powered exoskeleton (LLPE) is a human-machine system. It can follow the human movement and provide assistance for people who carry many. Generally, the anthropomorphic designing structure is used to realize the motion space coupling between the operator and the exoskeleton. In recent years, unpowered load-carrying parallel lower extremity exoskeleton (ULLPE) has been enormously studied. Compared with load-carrying lower limb powered exoskeleton, unpowered load-carrying lower extremity exoskeleton possesses merits such as smaller energy consumption, lighter weight, lower manufacturing cost, and higher stiffness, in addition to the inherent advantages of the general load-carrying lower limb powered exoskeleton in terms of bigger energy consumption, lower stiffness, higher manufacturing cost, and lower load to weight ratio. A novel ULLPE is the focus of the current trend in the research community, and various forms of LLPE have been presented.

In 1960, the first human exoskeleton (Hardiman) was developed by general motors and mainly used for easing the fatigue of soldiers in USA. But it has a heavy body, a large volume, and only a single powered arm. In the 2000s, BLEEX [1], which was designed at the University of California, is to make exoskeleton easier for wearers to carry heavy objects. A military-assisted exoskeleton called HULC [2] which comprised an external driven motor was produced in the Berkeley bionic technology company in 2009. It can assist the human body to run at the speed of 11km/h at a negative weight of 90kg, but the endurance is short. In the 1980s, Cavagna, Kaneko, and others who were from Italy analyzed the body biomass utilization of different state of human walking and came to a conclusion that the energy that can be wasted during human walking is put forward to help the body walk. James Walsh et al. called the process human body energy storage strategy [3–7]; the progress can be described that, in the process of walking, the muscles can store part of gravitational potential energy and in the process of the human body movement next release walking load to reduce the human body. Human energy storage strategy can be used to make good use of the wasting energy of human muscle storage and walking, which is of great

significance for the improvement of human walking ability. Steven H. and others [8] designed an unpowered exoskeleton and some experiments were carried out to identify the results of theory. In 2016, Donghai et al. [9] presented the design and analysis of a passive body weight- (BW-) support lower extremity exoskeleton (LEE) with compliant joints to relieve compressive load in the knee. The new design fully used the energy of human muscle storage and walking and promoted the development of unpowered exoskeletons. Recently, the design, kinematic, and dynamic problems including position analysis, singularity analysis workspace, and force analysis of the exoskeleton have been investigated by Cuan-Urquizo [10]. Emmanouil Spyrakos Papastavridis introduced PDD and PPDD control schemes combined with gravity compensation, which have improved the development of strategies that permitted COMAN to achieve walking trajectories. Dongming Gan and Jian S. Dai proposed a unified inverse dynamics model of a metamorphic parallel mechanism with pure rotation and pure translation phases; their work mainly gives good optimal design and control of the mechanism designed by them in various applications using two phases. Besides these exoskeletons mentioned above, some other exoskeleton architectures can be found in the literature [11–15].

In this paper, a novel unpowered 8-DOF exoskeleton with four degrees of translational freedom and four degrees of rotational freedom is presented. It should be pointed out that seldom ULLPE can be designed in this way, this is also one novel contribution in this paper. The paper's structure is arranged as follows. Firstly, the structure characteristics and DOFs of this exoskeleton are analyzed based on analyzing the number of links and the kinematic joints in Sections 2 and 3, respectively. The workspace of the mechanism for the exoskeleton is obtained based on the forward position analysis in Section 4, and using computer code programming, several shapes of the reachable workspace of the exoskeleton are obtained in Section 5. Furthermore, the static performance analysis of the mechanism is analyzed by the balance force analysis between limbs in Section 6.1. Then, Section 6.2 presents the optimum stiffness of the spring for energy-restoring device by the genetic algorithm, and the static force of the supporting leg of the person who is not wearing the unpowered exoskeleton is gotten with the aim of comparing the changes of force and torque before and after wearing the exoskeleton in Sections 6.3 and 6.4, respectively. Lastly, Section 7 summarizes the full paper.

2. An Unpowered Exoskeleton and Its Structure Characteristics

As shown in Figure 1, the structure of the ULLPE which was formulated is of symmetry and the two legs both have the identical kinematic characteristics. Therefore, one of legs is taken as the study object. The proposed unpowered exoskeleton mainly comprised upper supporting plate, upper limb link, postsupporting link, connection link, energy-restoring part, and lower supporting plate. Here, meanwhile, as seen in Figures 2 and 3, the swing leg comprises two branches chains. A variable stiffness energy storage device with 12 parts is designed. The detailed structure is shown in Figure 2. Here,

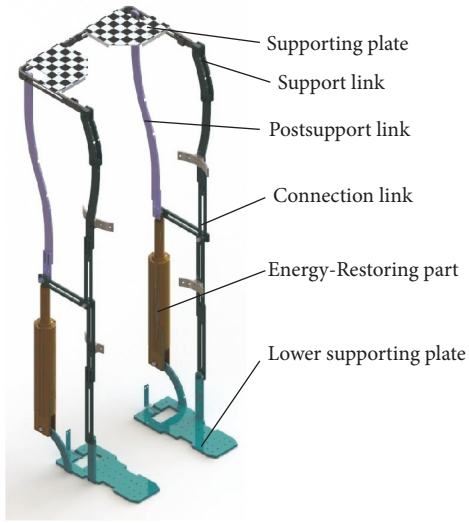

Figure 1: CAD model of the proposed unpowered exoskeleton.

upper cylinder link and the lower cylinder link form a moving pair, and the long spring with a large diameter and a small stiffness is installed at the inner wall of the lower connecting rod of the guide cylinder, and the short spring is set under the guide cylinder. The short spring guide rod crosses the short spring center with a large diameter and a large stiffness to fit with the guide bar block, so as to achieve the initial compression of the short spring and exert the pretightening force. The swing leg is analyzed and the schematic model of that is depicted in Figure 2. Considering the complex situation of the external exoskeleton, we restrict the working circumstance in the sagittal plane. As shown in Figure 1, we well know the comparison of the simple leg, such as the angle, knee, and the hip. The designation is satisfying the significant motions when people are walking. The swing leg has two branch chains: one is connected by *R- R- R- R* and the other by *R- R -CS- R*. Here, *R, CS* represent the revolute joint and energy-containing device. For the proposed mechanism, the structure with parallel topology is just moving in the sagittal plane and the CS can restore the energy which comes from the kinetic energy of individuals. It consists of two compressed springs and can lower the load of the load-carrying persons. Firstly, the schematic model of the swing leg is depicted in Figure 3. Locating the coordinate system *O-xy* attached to postsupporting with *O,* link OA_1 with the *x* axes is consistent with OA_1 and *y* axes are perpendicular to the OA_1 and *O* is the origins. The signs L_b, L_1, L_2, L_3, L_1, L_4, and L_5 represent the length of the lines OA_1, A_1A_2, A_2A_3, A_3A_4, and A_6A_3 respectively. The angles are expressed in Figure 3. It is important to note that β is the angle between the vector A_6A_3 and the vertical direction and β_1 between the vector A_6A_5 and the vertical direction.

3. Mobility Analysis

The degree of freedom of the mechanism is determined by the combined effect of the four limb constraint forces/couples.

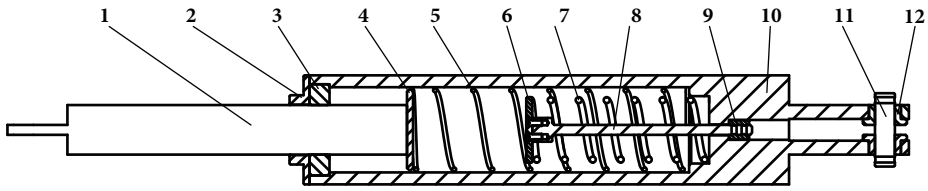

Figure 2: CAD model of the energy-storing device.

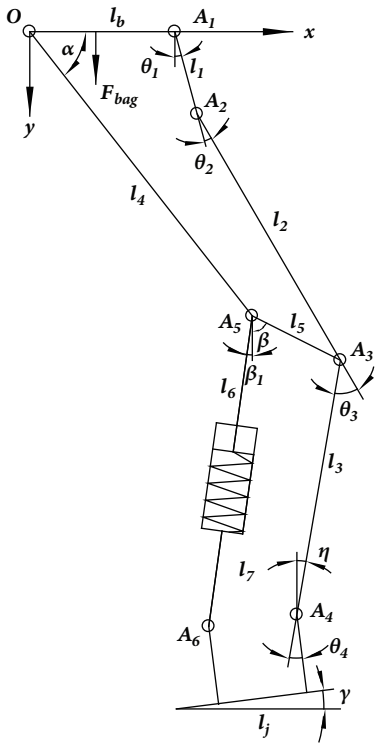

Figure 3: The schematic model of the swing leg.

In this paper, counting the number of the joints and links is used to analyze mechanism. As well-known for us, a link has 3 freedoms and revolute joint has one freedom in a simple plane. Here, a simplification for CS is taken to analyze the freedom. The CS can be considered as a prismatic joint and has one translational degree.

$$F = \sum_{i=1}^{p} i * p_i - L * \lambda_i \tag{1}$$

Here, L=p-n+1, n denotes the number of the links, p represents the number of the freedoms of every joint, and i is the code of the link, respectively.

From (1), according to the analysis of the mechanism concerning the swing leg, $n = 9, \lambda = 3, p = 10$, we can see that the swing leg limb owns 4 degrees. Considering the complex of the exoskeleton and in order to simplify the analysis, here, we take the hip link as the static link. As depicted in Figure 2, the number of the links has 9 links, and the amounts of revolute joints are 8 and being seen as a prismatic joint. So according to formula (1), the degree of freedom of the swing leg is 4; therefore, the ULLPE has 8 degrees. So, the simple leg owns two degrees of rotational freedom and two degrees of translational freedom.

4. Forward Position Analyses

The forward position analysis of the swing leg is concerned with ensuring the angle pose given the limb lengths. Initially, drawing the schematic model of the swing leg, the position of swing leg concerning the sagittal plane is obtained by using closing-vector-circle method. Here, the coordinates of the center of the knee are (x, y), and the coordinates of the center of the ankle are (x_1, y_1). The expressions can be described with the closed loop method:

$$\overrightarrow{OA_3} = \overrightarrow{OA_1} + \overrightarrow{A_1A_2} + \overrightarrow{A_2A_3} \tag{2}$$

$$\overrightarrow{OA_3} = \overrightarrow{OA_6} + \overrightarrow{A_6A_3} \tag{3}$$

The formulas can be rewritten as follows:

$$\left\|OA_6A_3\right\|_x = l_b + l \times \sin(\theta_1) + l_2 \times \sin(\theta_2 + \theta_1) \tag{4}$$

$$\left\|OA_1A_2A_3\right\|_x = l_4 \times \cos(\alpha) + l_5 \times \sin(\beta) \tag{5}$$

$$\left\|OA_1A_2A_3\right\|_y = l_4 \times \sin(\alpha) + l_5 \times \cos(\beta) \tag{6}$$

$$\left\|OA_6A_3\right\|_y = l_1 \times \cos(\theta_1) + l_2 \times \cos(\theta_1 + \theta_2) \tag{7}$$

Meanwhile, according to Figure 3, $L_5 is$ a constant, so the constrain condition can be depicted as follows:

$$\left\|A_6A_3\right\| = l_5 \tag{8}$$

According to (2)-(8), the coordinates of the angle and knee can be ensured.

$$\cos(\alpha) = \left(l_b + l_1 \times \sin(\theta_1) + l_2 \times \sin(\theta_1 + \theta_2)\right) \frac{1}{l_4} \tag{9}$$

$$\sin(\beta) = (A - B) \frac{1}{l_5} \tag{10}$$

Here,

$$\begin{aligned} A &= l_b + l_1 \times \sin(\theta_1) + l_2 \times \sin(\theta_1 + \theta_2) \\ B &= l_1 \times \cos(\theta_1) + l_2 \times \cos(\theta_1 + \theta_2) \end{aligned} \tag{11}$$

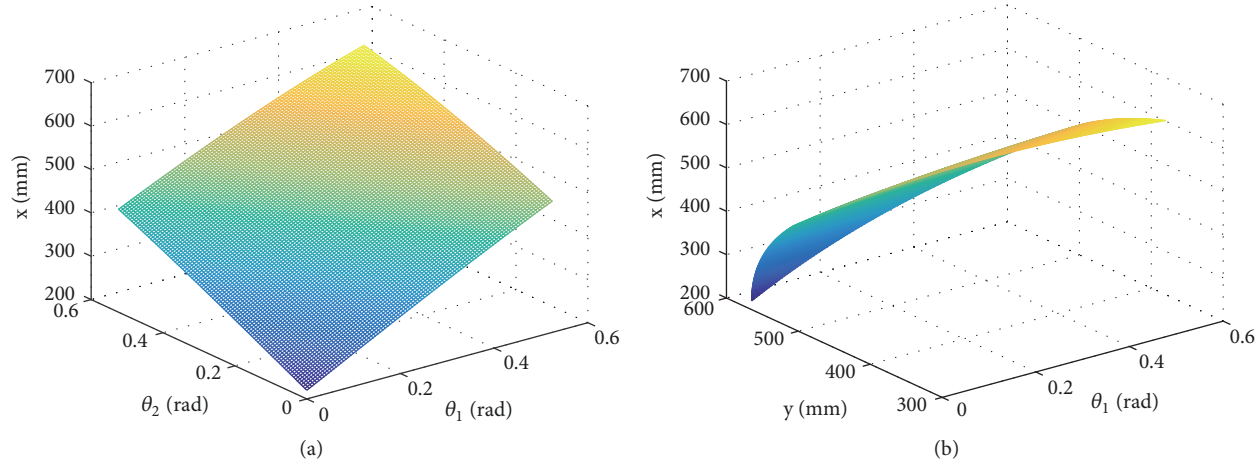

Figure 4: The reachable workspace of the knee joint concerning the swing leg.

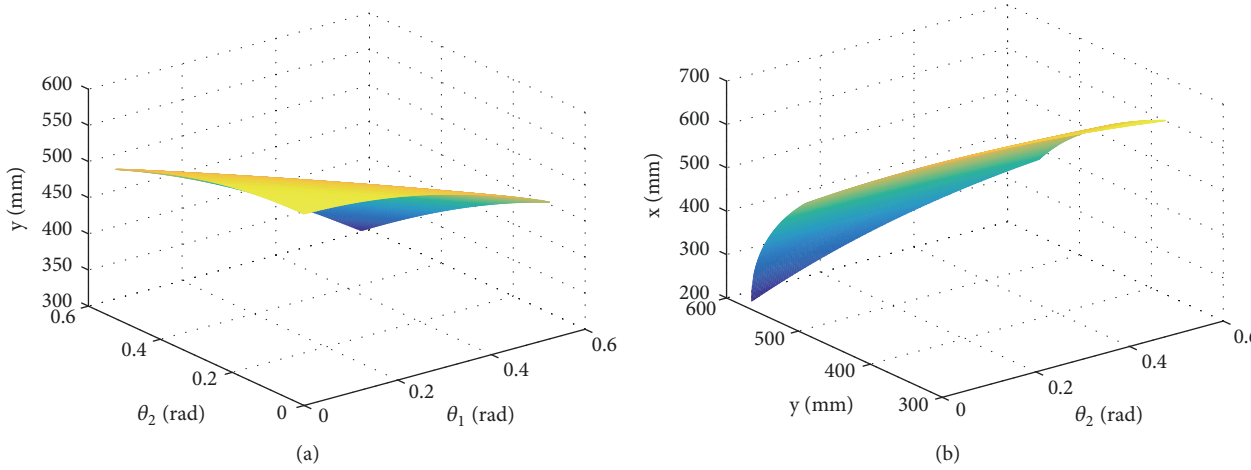

Figure 5: The reachable workspace of the knee joint concerning the swing leg.

The pose of the knee is depicted as follows:

$$x = l_b + l_1 \times \sin(\theta_1) + l_2 \times \sin(\theta_1 + \theta_2) \tag{12}$$

$$y = l_1 \times \cos(\theta_1) + l_2 \times \cos(\theta_1 + \theta_2) \tag{13}$$

So, the coordinates of the angle in the sagittal plane can be described as follows:

$$x_1 = l_b + l_1 \times \sin(\theta_1) + l_2 \times \sin(\theta_1 + \theta_2) + l_3 \times \sin(\theta_3 - \theta_1 - \theta_2) \tag{14}$$

$$y_1 = l_1 \times \cos(\theta_1) + l_2 \times \cos(\theta_1 + \theta_2) + l_3 \times \cos(\theta_3 - \theta_1 - \theta_2) \tag{15}$$

According to formulas (2)-(14), we can see that, for the proposed ULLPE in this paper, the forward position analyses of the mechanism can be calculated directly though analytical method; the location of the joints for the knee and ankle, which is enormously significant for doing some research in workspace, can be obtained.

5. Workspace Analysis

In this section, the workspace of the swing leg and the reachable workspace of the simple ULLPE are obtained based on the forward position analysis. From Section 4, we can see that given a set of limb rotations angles (θ_1 θ_2 θ_3), the other parameters including pose coordinates can be calculated directly by corresponding equations. So, when the restrictions to the link rotation angles are set up, the swing leg motion workspace and the reachable workspace of the mechanism can be obtained. Here, the workspace of the knee joints and the angle joints are analyzed, respectively.

5.1. Case Studies on the Workspace of the Knee Joint and Ankle Joint. In order to explore the relationships between the series of parameters and the mechanism, we define some parameters values. The architectural parameters of the ULLPE exoskeleton are selected as l_b=100 mm, l_1=300 mm, l_2=500 mm, l_3= 600 mm, l_4= 550 mm, l_5= 150 mm,0≤ θ_1 ≤pi/4, 0≤ θ_2 ≤pi/4, and θ_3=pi/4. Here, the spectrum of the knee concerning the leg is depicted in the Figures 4(a), 4(b), 5(a),

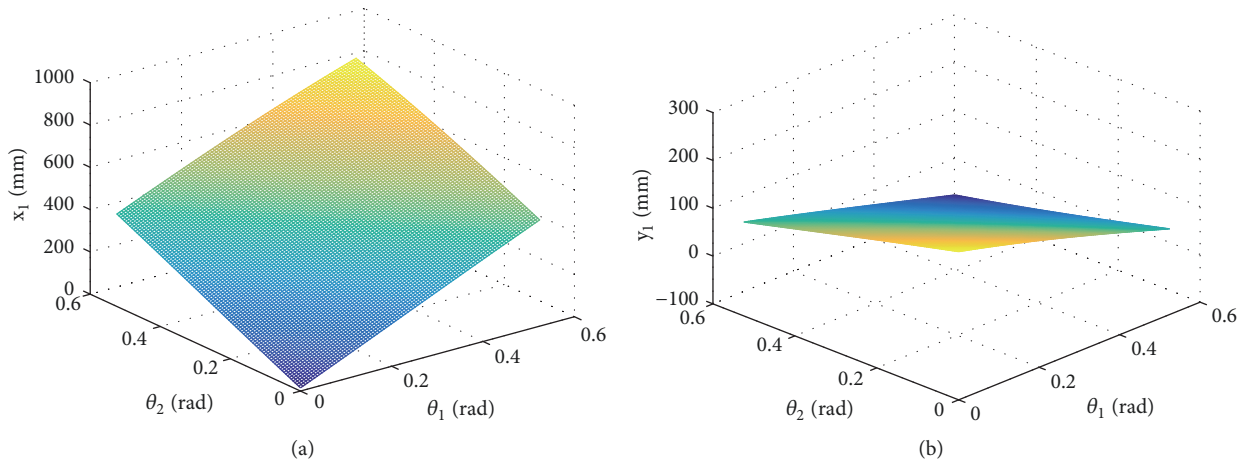

Figure 6: The reachable workspace of the ankle joint concerning the swing leg.

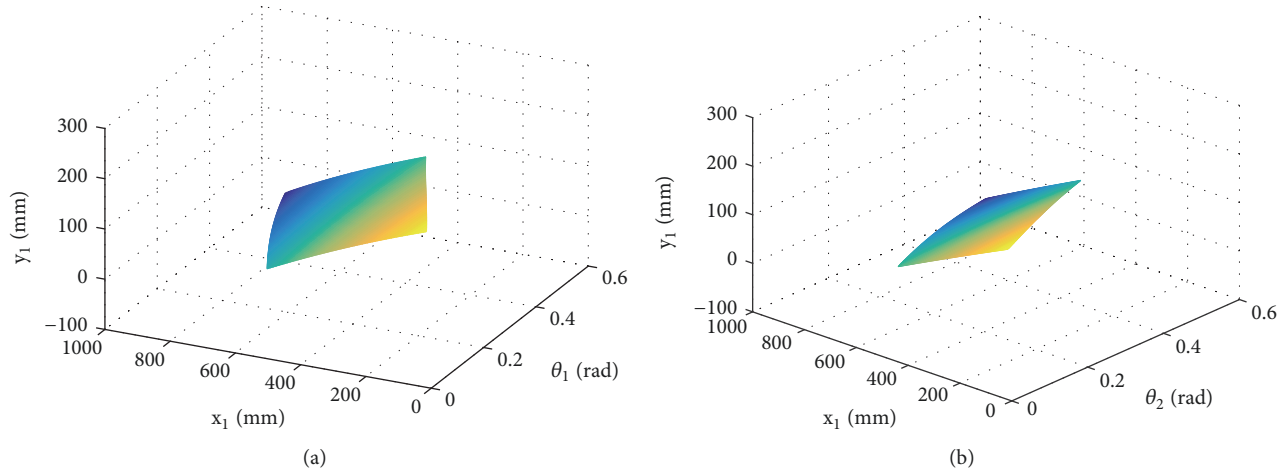

Figure 7: The reachable workspace of the ankle joint concerning the swing leg.

and 5(b). The workspace of the manipulator can be generated by a MATLAB program. The reachable workspace of the ankle for the exoskeleton is shown in Figures 6(a), 6(b), 7(a), and 7(b).

According to given the parameter and the simulation, Figures 5, 6, and 7 show us the basic shape concerning the swing leg. The reachable workspace of the swing leg can be seen from the above images.

5.2. Case Studies on the Workspace of the Swing Leg for the Exoskeleton. The approach followed in this paper for having an insight into the reachable workspace of the swing leg considers the workspace of the knee and angle joints and the distribution between each parameter. Figures 4 and 5 show that the distribution of y and x only has relation with the θ_1 and θ_2, regardless of the variation of θ_3. Figures 6 and 7 depict that the distribution of y_1 and x_1 only has relation with the θ_1 and θ_2, regardless of the variation of θ_3. Figure 8 demonstrates that the distribution of y_1 and x_1 only has relation with the y and x, and the parameters, including all the values of the y and x and y_1 and x_1, are altogether exhibited in the three-dimensional space.

6. The Spring Stiffness Optimization on Exoskeleton

In this section, the stiffness of spring is acquired to optimize for enhancing the function of the exoskeleton performance. Firstly, the analysis of the supporting leg for the exoskeleton is worked out based on the static force analysis between links. Secondly, the conditions of stiffness constrain are listed. The most reasonable stiffness of the spring for the energy-storing is obtained. Thirdly, in order to make a comparison of force and torque before and after wearing exoskeletons, we make an analysis on our body and draw some equations when we do not wear it. Finally, some variation curves are shown by software. Meanwhile, some conclusions are carried out.

6.1. Calculation of Joint Torque on Exoskeleton. The description of the forces exerted on every limb for supporting leg is shown in Figure 9.

From Figure 9, the force direction exerted every limb can be seen. According to the balance of the whole exoskeleton

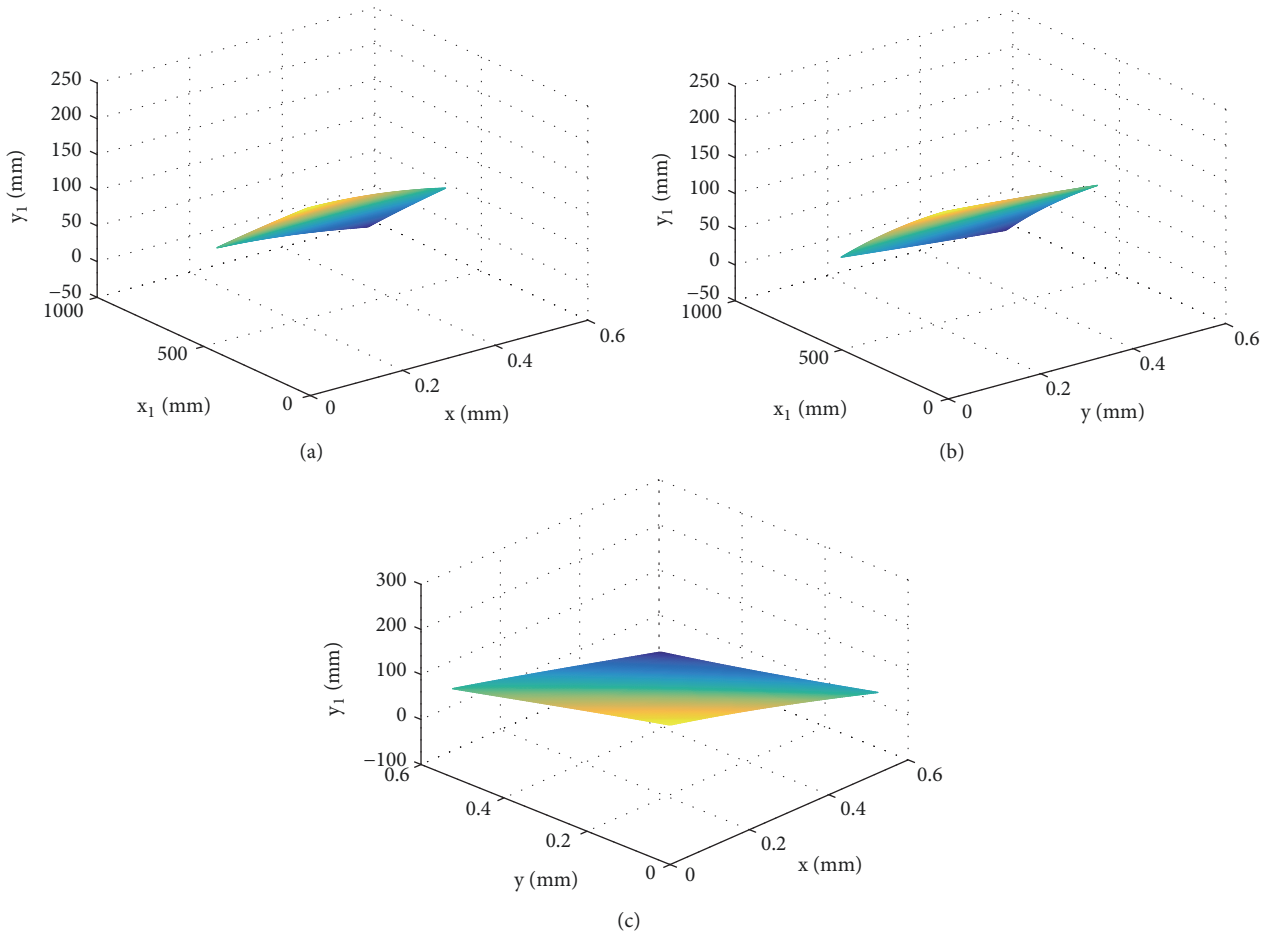

Figure 8: The distribution of the parameter concerning x, x_1, y, and y_1.

structure, the equations can be obtained and listed as follows:

$$\begin{aligned} \alpha_3 &= 180^\circ - \beta_1 - \beta, \\ \alpha_2 &= 90^\circ + \beta_1 - \alpha, \\ F_6 &= F_5 = K \times (l_{kt} - l_{k1}) \end{aligned} \tag{16}$$

While the spring 2 is compressed, the force F_5 and F_6 can be rewritten as follows:

$$\begin{aligned} F_5 &= F_6 \\ &= K \times (l_{kt} - l_{k1}) + K_2 \times (l_{kt} - 2 \times l_{k1} + l_{k2} - h_2) \\ &\quad + l_2 \times K_2 \end{aligned} \tag{17}$$

$$\begin{aligned} F_0 &= F_5 \times \frac{\sin(\alpha_3)}{\sin \pi (\alpha_2 + \alpha_3)}, \\ F_9 &= \frac{\sin(\alpha_2)}{\sin \pi (\alpha_2 + \alpha_3)} \times F_5, \\ F_{1x} &= F_0 \times \cos(\alpha) \end{aligned} \tag{18}$$

$$\begin{aligned} F_{bag} &= F_{1y} + F_0 \times \sin(\alpha), \\ F_{1x} &= F_{2x} = F_{3x} = F_{4x}, \\ F_{1y} &= F_{2y} = F_{3y} = F_{4y} \end{aligned} \tag{19}$$

Here, F_{bag}, F_z, F_m represent the weight of the bag, ground support force, and the friction from the ground, respectively.

Based on (17), (18), (19), and (20), the torques from each joint can be calculated

$$M_1 = F_{bag} \times l_b - F_0 \times l_b \times \sin(\alpha) \tag{20}$$

$$M_2 = M_1 + \left(F_{1y} \times \sin(\theta_1) + F_{1x} \times \cos(\theta_1)\right) \times l_1 \tag{21}$$

$$M_3 = M_2 + \left(F_{2y} \times \sin(\varepsilon) + F_{2x} \times \cos(\varepsilon)\right) \times l_2 \tag{22}$$

$$\begin{aligned} M_4 = M_3 + \big(&F_{3x} \times \cos(\eta) - F_{3y} \times \sin(\eta) - F_{9x} \\ &\times \sin(\beta) \times \cos(\eta) + F_{9y} \times \cos(\beta) \times \sin(\eta)\big) \times l_3 \end{aligned} \tag{23}$$

Here, $\eta = \theta_3 - \theta_2 - \theta_1$, $\varepsilon = \theta_2 + \theta_1$, $\gamma = 0^\circ$, l_b is the distance between the mass center of the bag and the human body, and K_1, K_2 are the two spring's stiffness, respectively.

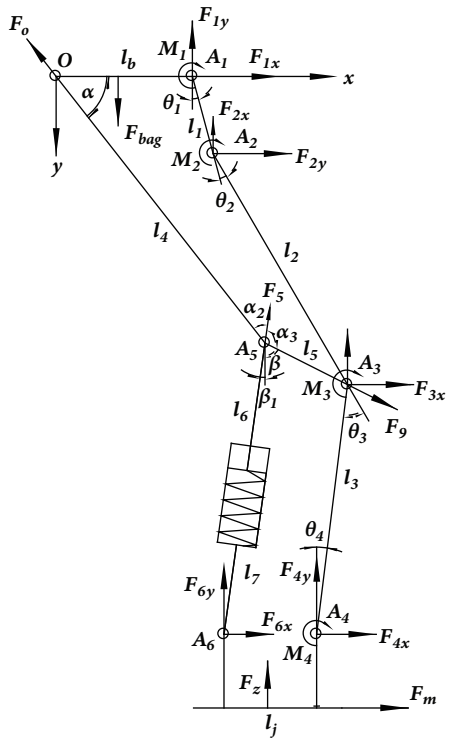

Figure 9: Forces analysis of every limb on the supporting leg.

6.2. Simulation Conditions, Parameter Settings, and Optimization Results. Here, while optimizing the spring stiffness, it should also meet the following constraints:

(1) The stiffness of the spring is bigger than zero.

(2) During a gait cycle, the torque of the knee joint should be lowered after optimization.

(3) The torque of the lumbar joint is always positive.

The constrain conditions can be described by some equations:

$$f(k) = \sum_{i=1}^{n} \left(\left| \frac{M_{1i}}{n} \right| + \left| \frac{M_2}{n} \right| + \left| \frac{M_3}{n} \right| + \left| \frac{M_4}{n} \right| \right) \quad (24)$$

$$\begin{aligned} \min \quad & (f(k)) \\ & K_1 > 0, \\ & K_2 > 0, \\ & M_1 > 0 \\ & M_{b2} > \mathrm{M}_{f2}, \end{aligned} \quad (25)$$

T_{b2} indicates the torque provided by the knee joint in the previous support cycle, and T_{f2} stands for the torque offered by the knee in the last support cycle; *f(k)* is the sum of the finite torque which is from the human body within a gait cycle; here, a supporting cycle T is divided into N equipartition; N is just one of portions in a supporting cycle T. By adding up all the effective torques applied to every moment of the whole support period, the total effective torque from the human body is acquired. By optimization, the effective torque is minimized by the human body in the support cycle of the whole gait.

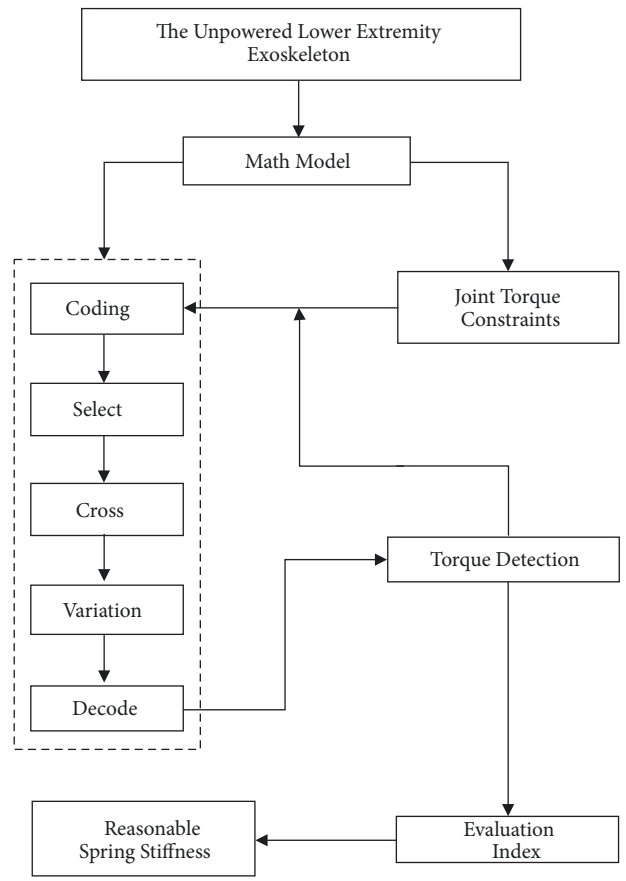

Figure 10: Optimization flowchart of the spring for energy-storing device.

The optimization of the stiffness of the exoskeleton spring can be optimized by adopting genetic algorithm. It is known that the pending unit is a variable stiffness energy storage element with pretightening force. It can compress only one spring in the early stage and the middle period of support, and two springs must be compressed at the last stage of support. The second spring is a large rigid spring with preload, and the optimized parameters are x_1 (k_1), $x_2(k_2)$, x_3 (l_{k2}), and x_4 (h_2). The MATLAB genetic algorithm optimization toolbox is used to solve the stiffness optimization model. The parameters of the toolbox are set as follows.

The number of population N_p=200, the maximum evolutionary algebra P_c=200, the cross-probability N_m=0.6, and the mutation probability N_m= 0.01, as shown in the objective function and constraint formulas (25) and (26). The layout optimization schematic diagram is shown in Figure 10.

By the optimization method proposed in the paper and with the help of the software (MATLAB), the optimal solution of the optimal parameter is obtained, as shown in Table 1.

6.3. Calculation of Joint Torque on Human Body. Similarly, as depicted in Figure 11, the coordinate system O_{xy} is established

Table 1: Optimal solution of optimal parameters.

K_1	K_2	l_{k2}	h_2
5.1 N/mm	7.0 N/mm	420 mm	28 mm

l_{k2} is the original length of spring 2, and h_2 is the initial compression quantity of spring 2.

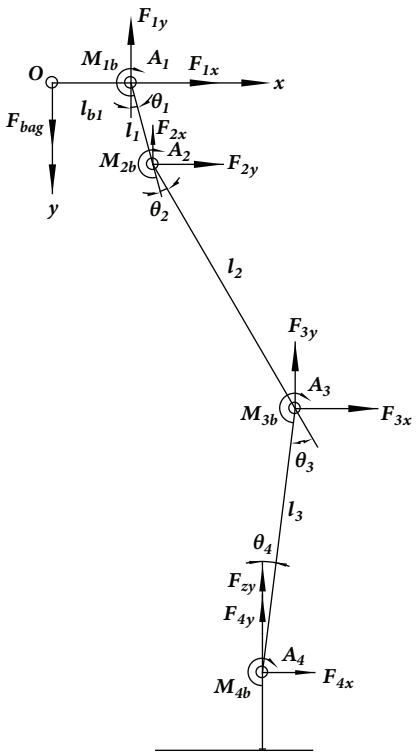

Figure 11: Pressure angles between each link.

at the origin of O, and the lower limb statics of human body is as follows:

$$F_{1x} = 0 \tag{26}$$

$$F_{1y} = F_{bag} = F_{zy}$$

$$F_{1y} = F_{2y} = F_{3y} = F_{4y} \tag{27}$$

$$F_{1x} = F_{2x} = F_{3x} = F_{4x}$$

Among them, F_{bag} is the weight of the load, and l_{b1} and l_1~l_3 are the distance from the load center to the human body and the length of the human body segments, respectively. F_{zy} is the counterforce of the support side.

The torque is provided by the joints of the human body.

$$M_{1b} = F_{bag} \times l_{b1},$$

$$M_{2b} = M_{1b} + F_{bag} \times l_1 \times \sin(\theta_1) \tag{28}$$

$$M_{3b} = M_{2b} + F_{bag} \times l_2 \times \sin(\varepsilon) \tag{29}$$

$$M_{4b} = M_{3b} + F_{bag} \times l_3 \times \sin(\eta) \tag{30}$$

where M_{1b}~M_{4b} represents the torque provided by the waist, hip, knee, and ankle joints from human body. θ_1~ θ_3 represents the motion angles of the human lower extremities, and $\theta = \theta_3 - \theta_2 - \theta_1$, $\varepsilon = \theta_1 + \theta_2$.

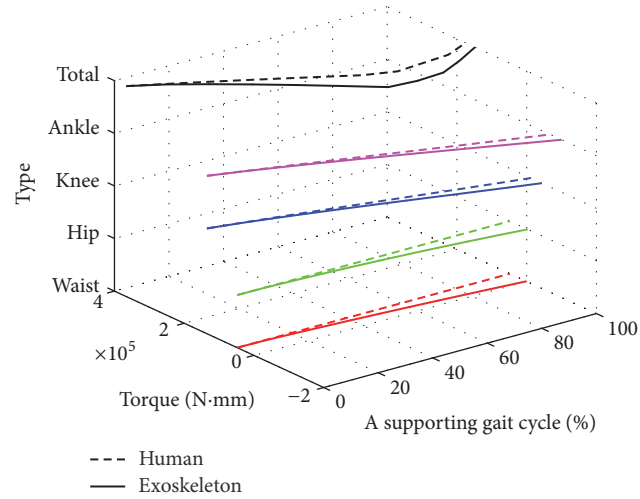

Figure 12: Comparison of joint torque before and after wearing exoskeleton.

6.4. Comparative Torque Analysis before and after Wearing. The torque applied to the waist, hip, knee, and ankle joints in a support period is calculated according to the formulas when the human body is not wearing the exoskeleton. In order to compare joint torque before and after wearing exoskeleton the torque provided by the human body's waist, hip, knee, and ankle joints is calculated when the human body is wearing the exoskeleton. During the entire gait support cycle and before and after wearing the exoskeleton, the torques provided by the waist, hips, knees, and ankle joints are compared (the torque is negative, which is indicating that the human joints provide the reverse direction torque). The average value of the torque applied to each joint of the human body during the entire gait support period is obtained, and the total effective torque exerted on each joint of the human body is also obtained. According to calculation in a supporting gait cycle, the waist and hip joint torques were reduced by about 42% and 40%, and the knee joint torque was reduced by about 3%, but the ankle joint torque was slightly increased about 9%. The total effective torque of the lower limb joints for the human body can be reduced by 16% when the exoskeleton is on load. The comparison of joint torque before and after wearing exoskeleton is depicted in Figure 12. The hip, waist, knee, and ankle joint torque saving ratio in a supporting gait cycle are shown in Figures 13–16. At the same time, the total torque savings in a supporting gait cycle are shown in Figure 17.

7. Conclusions

This paper proposes a novel unpowered lower extremity 8-DOF exoskeleton. Initially, the degree of freedom on the mechanism is ensured by analyzing the number of links and kinematic pairs. Then, according to the schematic diagram of the mechanism, the forward position analysis of the structure is carried out, such as the motion expressions of

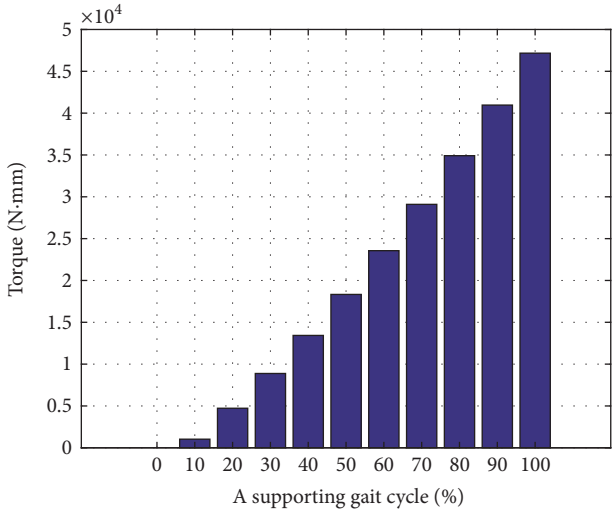

Figure 13: Waist joint torque saving ratio.

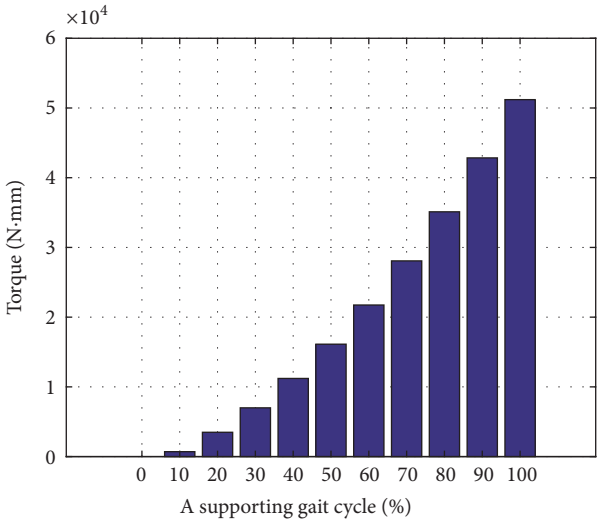

Figure 14: Hip joint torque saving ratio.

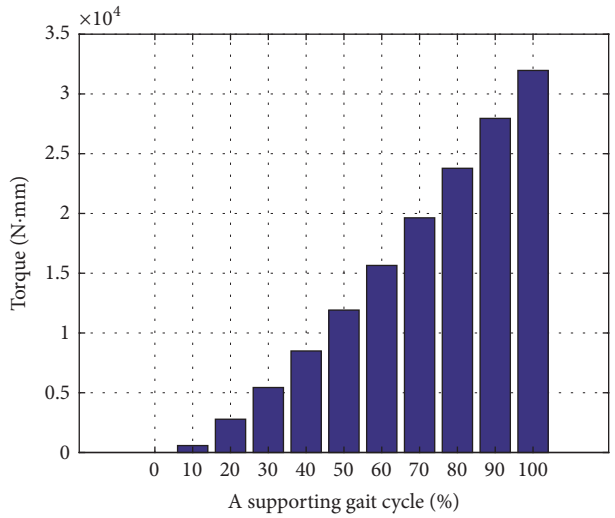

Figure 15: Knee joint torque saving ratio.

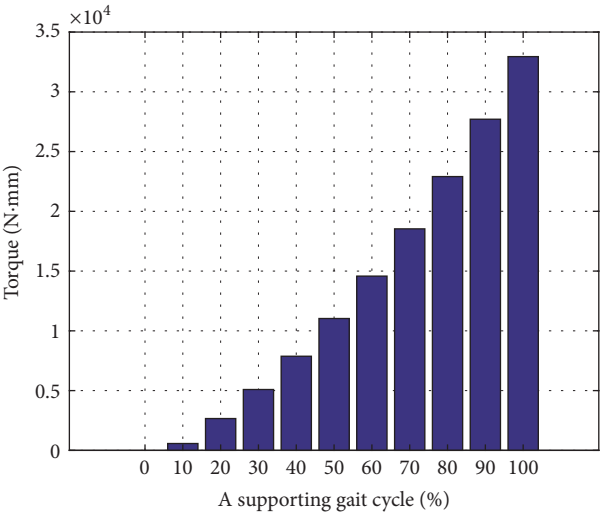

Figure 16: Ankle joint torque saving ratio.

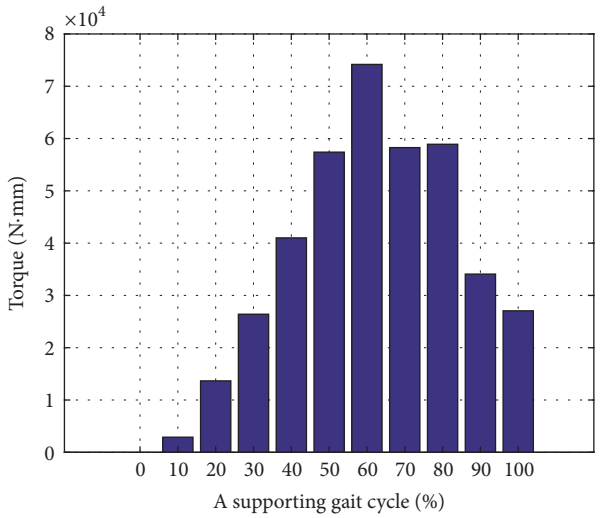

Figure 17: Total torque savings in a supporting gait cycle.

the knee and ankle joints. Then, based on these equations, the workspace of the knee and ankle is described by the software of MATLAB. Thirdly, in order to improve the performance of the exoskeleton, two springs of energy-restoring device in the mechanism are optimized by adopting genetic algorithm. So, the most suitable stiffness is acquired. Finally, the static force of the supporting leg for the person who is not wearing the unpowered exoskeleton is gotten with the aim of comparing the changes of force and torque before and after wearing the exoskeleton; meanwhile, some conclusions are drawn. Based on the kinematics analysis of the mechanism, the inverse/forward dynamics analyses, the stiffness performance analysis, and the other kinematic optimization of the mechanism will be investigated in the future work.

Data Availability

The data used to support the findings of this study are available from the corresponding author upon request.

Conflicts of Interest

The authors declare that they have no conflicts of interest.

Acknowledgments

This work was supported by the National Natural Science Foundation of China (NSFC) (Grant no. 51175144) and the Tian Jin Natural Science Foundation of China (TJSFC) (Grant no. 17JCZDJC40200).

References

[1] H. Kazerooni, R. Steger, and L. Huang, "Hybrid control of the Berkeley Lower Extremity Exoskeleton (BLEEX)," *International Journal of Robotics Research*, vol. 25, no. 5-6, pp. 561–573, 2006.

[2] N. L. Tagliamonte, F. Sergi, G. Carpino, D. Accoto, and E. Guglielmelli, "Human-robot interaction tests on a novel robot for gait assistance," in *Proceedings of the 2013 IEEE 13th International Conference on Rehabilitation Robotics (ICORR '13)*, pp. 24–26, IEEE, USA, June 2013.

[3] G. A. Cavagna and M. Kaneko, "Mechanical work and efficiency in level walking and running," *The Journal of Physiology*, vol. 268, no. 2, pp. 467–481, 1977.

[4] S. Mochon and T. A. McMahon, "Ballistic walking," *Journal of Biomechanics*, vol. 13, no. 1, pp. 49–57, 1980.

[5] H. Geyer, A. Seyfarth, and R. Blickhan, "Compliant leg behaviour explains basic dynamics of walking and running," *Proceedings of the Royal Society B: Biological Science*, vol. 273, no. 1603, pp. 2861–2867, 2006.

[6] K. Endo, D. Paluska, and H. Herr, "A quasi-passive model of human leg function in level-ground walking," in *Proceedings of the 2006 IEEE/RSJ International Conference on Intelligent Robots and Systems (IROS '06)*, pp. 4935–4939, IEEE, Beijing, China, October 2006.

[7] C. J. Walsh, K. Endo, and H. Herr, "A quasi-passive leg exoskeleton for load-carrying augmentation," *International Journal of Humanoid Robotics*, vol. 4, no. 3, pp. 487–506, 2007.

[8] S. H. Collins, M. B. Wiggin, and G. S. Sawicki, "Reducing the energy cost of human walking using an unpowered exoskeleton," *Nature*, vol. 522, pp. 212–215, 2015.

[9] D. Wang, K.-M. Lee, and J. Ji, "A Passive Gait-Based Weight-Support Lower Extremity Exoskeleton with Compliant Joints," *IEEE Transactions on Robotics*, vol. 32, no. 4, pp. 933–942, 2016.

[10] R. Di Gregorio, "The 3-RRS wrist: A new, simple and non-overconstrained spherical parallel manipulator," *Journal of Mechanical Design*, vol. 126, no. 5, pp. 850–855, 2004.

[11] W. Xu and Y. Li, "Kinematics and workspace analysis for a novel 6-PSS parallel manipulator," in *Proceedings of the 2013 IEEE International Conference on Robotics and Biomimetics (ROBIO '13)*, pp. 1869–1874, Shenzhen, China, December 2013.

[12] Y. Yun and Y. Li, "A general dynamics and control model of a class of multi-DOF manipulators for active vibration control," *Mechanism and Machine Theory*, vol. 46, no. 11, pp. 1549–1574, 2011.

[13] Q. Yan, B. Li, Y. Li, and X. Zhao, "Comparative study of two 2-RPU1-SPR parallel manipulators," in *Proceedings of the 12th World Congress on Intelligent Control and Automation (WCICA '16)*, vol. June 2016, pp. 1975–1980, Guilin, China.

[14] Q. Yan, B. Li, Y. Li, and X. Zhao, "Comparative stiffness analysis of two over-constrained manipulators," in *Proceedings of the 2016 International Conference on Advanced Robotics and Mechatronics, ICARM 2016*, pp. 225–230, Macau, China, August 2016.

[15] Qiang Yan, Bin Li, Yangmin Li, and Xinhua Zhao, "Kinematics comparative study of two overconstrained parallel manipulators," *Mathematical Problems in Engineering*, vol. 2016, Article ID 5091405, 12 pages, 2016.